

**ICSO 2016**

**International Conference on Space Optics**

Biarritz, France

18–21 October 2016

*Edited by Bruno Cugny, Nikos Karafolas and Zoran Sodnik*



***Fine guidance sensor/near-infrared imager and slitless spectrograph on James Webb Space Telescope: pupil alignment methodology and metrology***

*M. Maszkiewicz*

*N. Rowlands*

*D. Aldridge*

*A. Beaton*

*et al.*



icso proceedings



International Conference on Space Optics — ICSO 2016, edited by Bruno Cugny, Nikos Karafolas, Zoran Sodnik, Proc. of SPIE Vol. 10562, 1056223 · © 2016 ESA and CNES  
CCC code: 0277-786X/17/\$18 · doi: 10.1117/12.2296043

## FINE GUIDANCE SENSOR/NEAR-INFRARED IMAGER AND SLITLESS SPECTROGRAPH ON JAMES WEBB SPACE TELESCOPE - PUPIL ALIGNMENT METHODOLOGY AND METROLOGY

M. Maszkiewicz<sup>1</sup>, N. Rowlands<sup>2</sup>, D. Aldridge<sup>2</sup>, A. Beaton<sup>2</sup>, S. Delamer<sup>2</sup>, Sheng-Hai Zheng<sup>2</sup>, R. Ohl<sup>3</sup>  
and P. Coulter<sup>3</sup>

<sup>1</sup>Canadian Space Agency, 6767 route de L'Aéroport, Saint-Hubert, Canada, QC J3Y 8Y9, Canada,  
[michael.maszkiewicz@canada.ca](mailto:michael.maszkiewicz@canada.ca)

<sup>2</sup>COM DEV International Systems, Canada,  
[neil.rowlands@comdev.ca](mailto:neil.rowlands@comdev.ca), [david.aldrige@comdev.ca](mailto:david.aldrige@comdev.ca), [alexander.beaton@comdev.ca](mailto:alexander.beaton@comdev.ca),  
[sandra.delamer@comdev.ca](mailto:sandra.delamer@comdev.ca), [sheng-hai.zheng@comdev.ca](mailto:sheng-hai.zheng@comdev.ca)

<sup>3</sup>NASA Goddard Space Flight Centre, US,  
[raymond.g.ohl@nasa.gov](mailto:raymond.g.ohl@nasa.gov), [phillip.coulter@nasa.gov](mailto:phillip.coulter@nasa.gov)

### I. INTRODUCTION

The JWST is an international collaboration among the NASA, the European Space Agency (ESA), and the Canadian Space Agency (CSA). It is a large (6.5 m primary mirror diameter), infrared (0.6-27  $\mu\text{m}$ ) observatory that will study the first galaxies of the early Universe, the birth of stars and protoplanetary systems as well as exoplanets [1]. In 2018 the telescope will be launched to orbit the Sun-Earth Lagrange2 point, 1.5 million km away. The JWST architecture consists of three main elements; the Optical Telescope Element (OTE), the Integrated Science Instrument Module (ISIM), and the spacecraft element. The suite of the scientific instruments (SI) carried by the JWST are mounted in a common structure, the ISIM, which in turn is integrated with the OTE backplane. The instruments pick-off mirrors (POM) are in the close vicinity of the OTE focal surface, each relaying its assigned field of view (FOV) to the particular instrument and its detectors [2, 3].

### II. FGS/NIRISS FUNCTION

The large structure of the JWST requires a fine guidance system to achieve its intended image quality. For that purpose, its attitude control system is informed by a dedicated fine guiding sensor, the FGS. The FGS will produce a stream of guide star centroids that drive the OTE Fine Steering Mirror (FSM) which, together with the OTE tertiary mirror, is housed in the Aft Optical System (AOS). The movement of the FSM, located at the pupil of the OTE, will provide the line-of-sight pointing and stabilization.

The NIRISS is a multi-mode instrument that can be configured for broadband imaging, multi-object low-resolution slitless spectroscopy, high-contrast (interferometric) imaging and cross-dispersed spectroscopy optimized for exoplanet transit work. The more detailed description of the FGS/NIRISS functionality and design is provided in [4].

### III. PUPIL ALIGNMENT IMPORTANCE

There are several reasons for the high accuracy pupil alignment requirement of the OTE and SIs:

#### A. Sensitivity Maximization

Vignetting is especially critical when it occurs at the apertures close to the pupil, reducing the instrument sensitivity across its whole FOV. The most basic mitigation of the problem is usually in the form of oversized apertures; but mass, size and other design constraints often place limits on this approach. On the JWST, typical aperture oversize is about 5% with the resulting requirement for the instrument's lateral pupil shear on the order of only 1%, as defined by the pupil center's displacement divided by the circumscribed, nominal OTE pupil diameter.

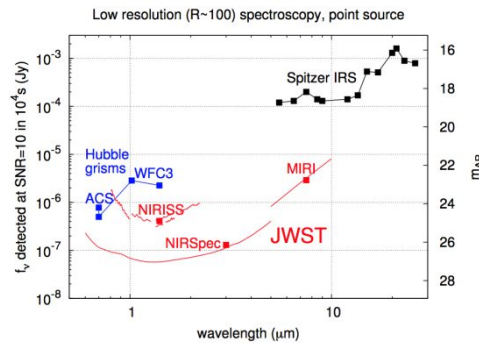


Fig.2. Faintest signal that can be detected at SNR=10 for a point source in  $10^4$  s. Fluxes are in units of Janskies and AB magnitudes. Source: *Space Telescope Science Institute*

Even with a sensitivity of few nJy ( $1 \text{ nJy} = 10^{-35} \text{ Watts/m}^2/\text{Hz}$ ), it is not expected that the JWST could detect an isolated first star. However, star or galaxy clusters are realistic targets. This view was recently [5] supported by a Hubble WFC3 observation of the oldest and most distant galaxy GN-z11. It lies at only  $\sim 400$  Myr after the Big Bang and extends the previous redshift record by  $\sim 150$  Myr.

GN-z11 is unexpectedly luminous and with relatively large stellar mass for a galaxy at such an early time.

One can expect that the greater sensitivity of the JWST and its longer infrared range will enable finding the galaxies at even earlier times.

#### B. Efficient Coronagraphy and Aperture Masking Interferometry

Two of the JWST science instruments (NIRCam [6] and MIRI [7]) have coronagraphic imaging modes dedicated to exoplanet discovery. Its success is strongly dependent on Lyot masks efficiency blocking residual, diffracted stellar light from occulters. Pupil shear misaligns Lyot masks causing degradation of coronagraph performance by allowing diffracted light to reach the detectors.

The Aperture Masking Interferometry (AMI) on NIRISS [8] is another technique enabling high-contrast imaging. It converts the full aperture of the telescope into an interferometric array of pairs of sub-apertures. The resulting Point Spread Function (PSF) is Fourier transformed and processed to retrieve the input scene. Each of the seven NRM sub-apertures has a hexagon shape and the set of apertures need to be co-aligned to a few percent accuracy with the OTE primary mirror segments projection at the pupil.

#### C. Accurate Wavefront Sensing

The OTE will be folded to fit into an Ariane 5 fairing and then unfolded and aligned on orbit. The Wavefront Sensing and Control process [9] will assist in getting it fully aligned and keeping it at optimal configuration on orbit. The process relies on knowledge of the system's exit pupil distortion and amplitude function to generate accurate estimates for the system's wavefront error. Amplitude variability (caused by coatings non-uniformity and /or vignetting) is particularly important for achieving the required wavefront measurement accuracy.

#### D. Stray Light Suppression

The OTE is generally an open structure without major baffles, potentially allowing a particular stray light artifact that we call "rogue path." The path originates from outside of the OTE nominal FOV, skips its primary and secondary mirrors, travels over the outer edge of the FSM aperture and then goes straight to the science instrument POMs. To block this path, a precise overlap between the OTE FSM aperture, which closely coincides with OTE exit pupil location, and projection of the internal stops of the instruments has to be maintained [10].

A detailed stray light analysis showed that the rogue path does not have a significant impact upon the FGS and NIRISS instruments. There are no direct, specular "rogue" paths that will reach the detectors, and the propagation of diffuse light to the detectors is significantly attenuated.

## V. OTE/FGS/NIRISS PUPIL LOCATIONS AND CHARACTERISTICS

The OTE exit pupil is located in close proximity to the FSM. In the case of the FGS, the local aperture stop is the perimeter of the Three Mirror Assembly tertiary mirror with a pupil image that is tilted with respect to the mirror's axis. The pupil image is well-corrected only at the edge of the tertiary's aperture where a pupil fiducial, in the form of a small, triangular notch, is located. Its fiducial (Fig. 3) has the form of a machined "bump" feature with a pin hole on one of the pupil mask holders of the Pupil Wheel. (The Pupil Wheel (PW) together with the Filter Wheel forms the Dual Wheel (DW) mechanism holding NIRISS filters, grisms, masks and fiducials.) Because they are located at the edge of the pupils, the notch and bump images are not visible during the ISIM-level testing of the instruments after integration. For that reason, both instruments have a Pupil Alignment Reference (PAR). In case of FGS, its PAR (Fig. 3) is located at the center of the tertiary mirror where OTE primary mirror central obscuration is projected, so this region of the tertiary mirror will always stay dark while in operation. The FGS PAR is a small, flat, reflective disk with crosses and dots and is used during the ISIM-level tests at NASA GSFC. Similarly, NIRISS is equipped with the PAR (Fig. 3) which occupies one of the PW positions. Its sub-assembly consists of a reflective mirror and a holder that allows the mirror's accurate mounting on the PW.

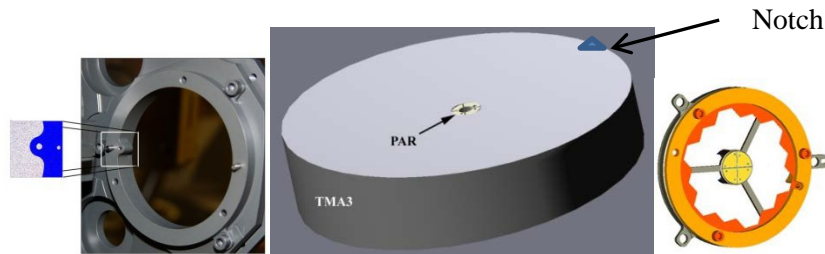


Fig.3. NIRISS bump and pin hole pupil fiducial in the Open Mask holder on the Pupil Wheel (left), FGS PAR machined onto the FGS tertiary mirror (middle) and NIRISS PAR (right).

## VI. FGS/NIRISS INTERFACES TO ISIM

A precise replication of the ISIM-to-FGS/NIRISS interface was achieved through the physical representation of the observatory coordinate system on the Ambient Science Instrument Mechanical Interface Fixture (ASMIF). A calibrated ASMIF was provided by GSFC and used to create the baseline measurements that connected alignments made during the FGS/NIRISS build back to the requirements of the OTE.

The ASMIF contained six titanium/Invar Science Instrument Interface Plates SIIPs which represented the FGS/NIRISS OB kinematic mount interfaces to the ISIM structure. The structure of ISIM provides structural support for ground testing and launch, and maintains the correct position of the science instruments with respect to each other and the OTE to very high precision. The ISIM structure is designed to distort very little during cool-down from room temperature to the cryogenic operating temperature and upon launch [11].

A verification of the repeatability of the SIIPs was done prior to the start of the assembly of the FGS/NIRISS. The mechanical assembly of the OB was verified using the alignment references provided by the ASMIF. The mechanical tolerances of the OB were also verified to create the required "datum" surface for the placement of the OB components of the FGS and NIRISS.

## VII. AMBIENT PUPIL ALIGNMENT

Ambient temperature pupil alignment of the FGS and NIRISS was the precursor to the cryogenic temperature alignment verification testing. The goal of this assembly and test phase was to align pupils to the predicted ambient locations with the assumption that they will move to their expected coordinates upon cooling to the cryogenic

operating temperature. The predicted ambient coordinates of the pupils were obtained from the overlaid “warm” optical and mechanical models of the instruments with orientation and position defined in 6 degrees of freedom (DOF). As almost all the FGS/NIRISS structure is made of Al-6061, the integrated CTE over 295 K--30 K for that material was used as a scale factor from cold to warm temperature. As described above, the pupil of the FGS is nominally determined by the notch at its tertiary mirror and for NIRISS by the bump and pin hole in the PW Clear Mask mount. For the ambient pupil alignment, the detectors and Fine Focusing Mirror (FFM) were removed from the FGS side. Following the removal of each component the datum locating pins for each component were measured, using the ASMIF as a coordinate reference. The ambient pupil shear test was then performed using back illumination of the FGS TMA and NIRISS Collimator TMA, projecting the instrument pupils on an auxiliary detector located at the OTE exit pupil location. The necessary pupil adjustments were then made by tip/tilt of the FGS and NIRISS POM and CFM, respectively. Once the ASMIF-based, ambient pupil shear requirement was satisfied, the POM and CFM were fixed by drilling and pinning, creating datum pin locations for each component.

The back illumination of the FGS pupil fiducial was accomplished using a fiber Pupil Back-Illumination Light (PBIL) placed at the instrument detector surfaces in the middle of the “warm” FOV location. Similarly, the Dual Wheel Illumination Backlight (DWIB) was used to illuminate the NIRISS pupil fiducial with its location behind the hole in the fiducial bump in the Open Mask holder (Fig. 3). The location of the pupil fiducial projection was facilitated by using the Pupil Alignment Target (PAT), a measurement tool which allowed measurement of the position of an optical image with respect to the Observatory coordinate system as represented by the ASMIF. This was achieved by positioning the PAT at the focal plane of the fiducial image and surveying it in 2-dimensions. The PAT was a square plate with a hollow square with inside knife edges. The position of the PAT can be adjusted in 6 DOF. Tooling holes on the PAT, including thru holes on the face, allowed its position and orientations to be measured using the laser tracker via metrology nests and spherically-mounted retro-reflectors.

At the DW assembly level, the NIRISS pupil fiducial location in the coordinate system defined by the ASMIF was established with the help of the external Pupil Datum Reference (PDF) and the Dual Wheel Alignment Reference (DAR). Both, the PDF and DAR were temporary, non-flight items. The relationship between the DAR tooling holes and the PDF and mask holders and mask pins was measured. These measurements transferred the geometry of the DW and PDF to the DAR. The DAR was then used as a positioning device on the OB.

## VIII ALIGNMENT TEST AT CRYO

The distance of about 3 m from the OTE exit pupil to the instruments’ focal surface and POMs precluded fitting the whole FGS/NIRISS assembly along with the pupil measuring system into the available TVAC chamber. The solution was to fold the light path using auxiliary mirrors. The concept is illustrated in Figures 4 and 5. In addition, the ASMIF had to be replaced by a Cryovac Test Fixture (CTF) capable of replicating the ISIM interfaces not only at ambient but also at operating temperature of 35 K (22 K survival). The design of the CTF included an aluminum frame and baseplate and an Invar plate providing final interface to the FGS/NIRISS KMs. All these three elements were allowed to “float” with respect to each other in the horizontal planes during cool-down, constrained only in rotation. Prior to pupil alignment, the CTF was surveyed at ambient to establish coordinate system. The unpopulated CTF then underwent extensive metrology characterization at the operating cryogenic temperature to establish its thermo-mechanical behavior and stability.

In the next step, the FGS/NIRISS was installed on CTF together with the fold mirrors, the Pupil Reference Light (PRL), and PBIL or DWIB.

The PRL was a fiber-fed telescope light source which produced a focusable round spot. It functioned as a pupil alignment reference datum for the pupil fiducial images formed by PBIL at ambient and operating temperatures. The PRL optical path (Fig.4) replicated the paths from the PBIL and DWIB outside the FGS and NIRISS, respectively, resulting in the PRL acting as a null device by cancelling the effect of any movement of the CTF components, especially the fold mirrors and imaging device. It was designed and manufactured to ensure that its optical and mechanical axes were as co-aligned as possible. In addition, the axes’ cool-down offset was measured during characterization of the PRL.

The imaging device for PRL spot and fiducials was a silicon sensor-chip assembly (SCA), described herein as a Read-out Integrated Circuit (ROIC). This sensor was the ROIC portion of the infrared detectors used in the instrument, which had the advantage of being able to image both in the visible and near-IR portion of the spectrum at ambient as well as at cryogenic temperatures, albeit with low effective quantum efficiency.

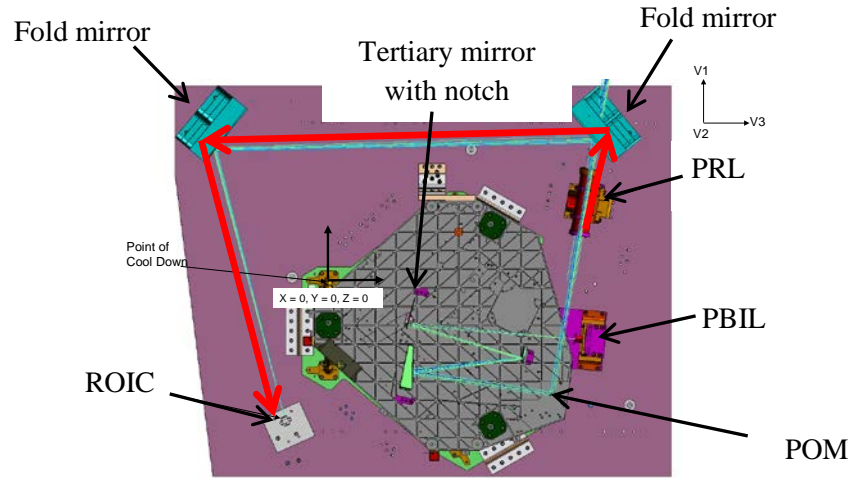


Fig.4. Cryo Test Fixture (FGS side) with folded optical path for tests at cryo. PBIL-FGS-Fold Mirrors-ROIC path shown in blue. PRL-Fold Mirrors-ROIC path shown in red.

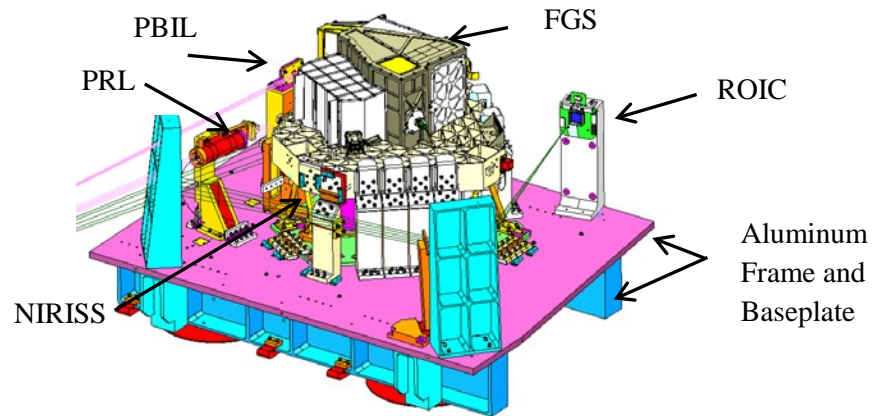


Fig.5. Cryo Test Fixture with FGS and NIRISS for cryo pupil alignment and test

In order to position the PRL spot and the pupil fiducials in the V-coordinate system at the “warm” OTE pupil location, one of the auxiliary fold mirrors was removed from its pins on the CTF baseplate, creating un-folded test configuration with images recorded again using PAT. At that stage, final POM and CFM corrections were performed for their desired orientations at ambient. To preserve the traceability and integrity of the interface to the ISIM structure, the position of the FGS pupil fiducial was compared to the ambient measurement on the ASMIF after ambient alignment. After that, the fold mirror was replaced and the locations of the FGS and NIRISS pupils measured in the folded configuration using ROIC. The ROIC location had been determined using as-built data for fold mirror orientations and then installed using the PAT device as a metrology tool. As in the case of the un-folded configuration, the ROIC

“warm” folded position on CTF had to ensure its correct location in the V-coordinate system at the operating temperature.

In the next step, the CTF was loaded into a TVAC chamber and cooled to the operating temperature. After reaching the test plateau and desired temperature profiles across the assembly (i.e., gradients less than 2 K), the PRL and PBIL on FGS side and DWIB on NIRISS side were illuminated and the positions of the PRL spot and fiducial images on the ROIC were measured.

Extensive metrology of the critical elements of the CTF and OB was carried out during cool-down and warm-up phases. The analysis of the results was supported by detailed Structural-Thermal and Optical (STOP) modeling, as well as error budgets, to predict and correlate the fiducial image locations at ambient and operational temperatures, as well to establish pass/fail criteria for shear.

After returning to ambient, all basic alignment parameters, like POM, CFM, PRL, PBIL, DWIB and ROIC orientations, as well as image locations, were measured again to assure that they remain within expected tolerances

## IX. PUPIL SHEAR ALIGNMENT ERROR BUDGETS

### A. Construction of Budgets

The FGS/NIRISS pupil shear error budgets have been constructed to provide an estimate of predicted performance errors of the instruments. The estimates were based on mechanical, assembly, test, and environmental factors. The optical performance errors were obtained from the optical modeling of the as-built instruments or their sub-systems. A bottom-up approach was used for estimating the uncertainties associated with the performance of the critical components of each instrument and their sensitivity to various factors.

#### B. Pupil Shear Error Contributors

The following environmental factors contributed to the pupil shear on-orbit error:

1. Error in the ROIC positioning with respect to the OTE pupil.
2. Error in the calculated interface translation between the ROIC and KMs at cryo.
3. ROIC stability in the TVAC chamber.
4. PRL spot movement from ambient to cryo.
5. Uncertainty in the gravity sag calculation (i.e., the 1g to 0g correction or “g-release”).
6. Misalignment of components (i.e., “non-common path” error) and movement of OB with respect to the OTE (i.e., “common-path” error) due to vibration.
7. Uncertainty in expected distortions over the operating temperature range.
8. Effect of the CFM movement across the required +/-3.1mm OTE defocus range.
9. Optical Bench and Optical Bench components vibrations.

The following measurement errors contributed to the pupil shear error:

1. Error in orientation to the V-coordinate system
2. Error in pupil fiducial image interpretation.
3. Error in PRL ambient image interpretation.
4. Error in PRL cryo image interpretation.
5. Error in the POM adjustment.
6. Error in the CFM and Pupil Wheel adjustment.
7. Repeatability of the Pupil Wheel positioning.

### C. On-Orbit FGS and NIRISS Pupil Shear Budgets

The top-level FGS and NIRISS pupil shear budgets are shown in Tables 1 and 2 below.

Table 1. FGS pupil shear top level budget

Error Budget Item	Value (mm)	Estimated Pupil Shear at OTE (%)	Contribution	From
Cryo pupil alignment	1.64	1.08	subtotal	
Vibration	0.25	0.17	RSS	Analysis
Gravity Sag	0.04	0.02	RSS	Analysis
Environmental common path	0.26	0.17	RSS subtotal	
FGS Pupil Shear	1.66	1.09	Total	Measurement & Analysis

Table 2. NIRISS pupil shear top level budget

Error Budget Item	Value (mm)	Estimated Pupil Shear at OTE (%)	Contribution	From
Cryo pupil alignment	1.96	1.29	Subtotal	
OB vibration	0.25	0.17	RSS	Analysis
Gravity sag	0.06	0.04	RSS	Analysis
Environmental common path	0.26	0.17	RSS subtotal	
NIRISS pupil shear at nominal OTE focus	1.98	1.30	RSS subtotal	
DW position resolution	0.60	0.40	RSS	Analysis/measurement
CFM orientation for $\pm 3.1$ mm OTE defocus	1.22	0.80	RSS	Analysis/measurement
Operational factors causing shear	1.36	0.89	RSS subtotal	
NIRISS Pupil Shear	2.40	1.58	RSS Total	Measurement & Analysis

#### X. FGS/NIRISS TO ISIM INTEGRATION AND PUPIL ALIGNMENT TEST

The ISIM Element utilized another precision fixture to represent its interface to the OTE, the ISIM Test Platform (ITP). The ITP is an Invar platform that held the ISIM structure and science instruments and contains OTE-like interface features. The optical test and verification of the instruments at the ISIM-level was accomplished using a full-field, cryogenic optical stimulus, the OTE Optical Simulator (OSIM), inside the Space Environment Simulator (SES) TVAC chamber at GSFC. During these tests, each instrument's PAR was front-illuminated and imaged together with the overlapped OSIM PAR shadow. The ambient temperature images of the PARs and thermo-mechanical modeling were used to predict their locations with respect to the notch and bump fiducials at the operational temperature. Instrument and OSIM PAR calibration data were then used to calculate actual pupil coordinates resulting in the on-orbit shear values as in Table 3, including gravity release estimates. Ambient and cryo temperature ISIM pupil methodology and metrology is described in [10], [12], [13] and [14].

Table 3. Predicted FGS and NIRISS ISIM level on-orbit pupil shear values (gravity sag corrected)

	FGS	NIRISS
<b>Pupil Shear (on-orbit)</b>	<b>0.90%</b>	<b>1.56%</b>
<b>Uncertainty (1 <math>\sigma</math>)</b>	<b>0.42%</b>	<b>0.42%</b>

#### XI. ISIM (FGS/NIRISS) Integration to OTE

Before integrating with the OTE (spring of 2016), the ISIM was verified to meet with margin the requirements relative to its interface, so the ISIM KMs were not adjusted. Since all the SI pupil positions are now fixed with respect to each

other in the ISIM, the final science instruments pupil alignment verification will be conducted via NIRCcam pupil testing at the integrated OTE and ISIM (OTIS) level at NASA's Johnson Space Center in Houston in 2017.

#### Acknowledgment

The authors would like express they appreciation to Clinton Evans (ComDev, retired) for his great contribution regarding alignment concept and testing of the FGS/NIRISS.

#### References

- [1] Gardner, J.P., John C. Mather, J.C., Clampin, M., Doyon, R., Greenhouse, M.A., Hammel, H.B., Hutchings, J.B., Jakobsen, P., Lilly, S.J., Long, K.S., Lunine, J.I., McCaughrean, M.J., Mountain, M., Nella, J., Rieke, G.H., Rieke, M.J., Rix, H.W., Smith, E.P., Sonneborn, G., Stiavelli, M., Stockman, H.S., Windhorst, Gillian, Wright, R.A S., Science with the James Webb Space Telescope, *Proc. SPIE* vol. 6265, 62650N, 2006.
- [2] Greenhouse, M.A. The JWST Science Instrument Payload: mission context and status, *Proc. SPIE*, vol. 9904, 2016.
- [3] Clampin, M. James Webb Space Telescope: The Road to First Science Observations, *Proc. SPIE*, vol. 9143, 2014.
- [4] Maszkiewicz M., Saad K., Rowlands N., Doyon R., Hutchings J.B, JWST Fine Guidance Sensor and Near-Infrared Imager and Slitless Spectrograph, in *Optical Payloads for Space Missions*, edited by Shen-En Qian, John Wiley & Sons Ltd., 2016.
- [5] Oesch P. A., Brammer G., van Dokkum P. G., Illingworth G. D., Bouwens R. J., Labbé I., Franx M., Momcheva I., Ashby M. L. N., Fazio G. G., Gonzalez V., Holden B., Magee D., Skelton R. E., Smit R., Spitler L. R., Trenti M., and Willner S. P., A Remarkable Luminous Galaxy at  $z=11.1$  Measured with Hubble Space Telescope Grism Spectroscopy, *The Astrophysical Journal*, 819:129 (11pp), 2016.
- [6] Green J.J., Beichman Ch., Basinger S.A., Horner S., Meyer M., Redding D.C., Rieke M., and Trauger J.T., High Contrast Imaging with the JWST NIRCAM Coronagraph, *Proc. SPIE*, vol. 5905, 2005.
- [7] Boccaletti A., Lagage P.-O., Baudoz P., Beichman C., Bouchet P., Cavarroc C., Dubreuil D., Glasse A., Glauser A. M., Hines D. C., Lajoie C.-P., Lebreton J., Perrin M. D., Pueyo L., Reess J. M., Rieke G. H., Ronayette S., Rouan D., Soummer R., and Wright G. S., The Mid-Infrared Instrument for the James Webb Space Telescope, V: Predicted Performance of the MIRI Coronagraphs, *PASP*, vol.127, p.623, 2015
- [8] Sivaramakrishnan, A., Lafrenière, D., K. E. Saavik Ford, K.E., McKernan, B., Cheetham, A., Greenbaum, A.Z., Tuthill, P.G., Lloyd, J.P., Ireland, M.J., Doyon, R., Beaulieu, M., Martel, A., Koekemoer, A., Frantz Martinache, F., Teuben, P., Non-redundant Aperture Masking Interferometry (AMI) and Segmented Phasing with JWST-NIRISS, *Proc. SPIE*, vol. 8442, 2012.
- [9] Acton D.S., Knight J.S., Contos A., Grimaldi S., Terry J., Lightsey P., Barto A., League B., Dean B., Smith J.S., Bowers Ch., Aronstein D., Feinberg L., Hayden W., Comeau T., Soummer R., Elliott E., M. Perrin M., Carl W. Starr C.W., Jr., Wavefront Sensing and Controls for the James Webb Space Telescope, *Proc. SPIE*, vol. 8442, 2012.
- [10] Bos, B.J., Ohl, R.G., and Kubalak, D. A., Pupil Alignment considerations for Large, Deployable Space Telescopes, *Proc. SPIE*, vol.8131, 2011.
- [11] Greenhouse M.A., Drury M P., Dunn J.L., Glazer S.D., Greville E., Henegar G., Eric L. Johnson E.L., Lundquist R.L., McCloskey J.C., Ohl R.G., Rashford R.A., and Voyton M.F., Status of the James Webb Space Telescope Integrated Science Instrument Module System, *The 2010 STScI Calibration Workshop*, Space Telescope Science Institute, 2010.
- [12] Coulter, Ph., Beaton, A., Gum, J.S., Hadjimichael, T., J., Hayden, J., E., Hummel, S., Hylan, J.,E., Madison, T., J., Maszkiewicz, Mclean, K., F., McMann, J., Melf, M., Miner, L., Ohl, R., G., Redman, K., Roedel, A., Schweiger, P., Te Plate, M., Wells, M., Wenzel, G., W., Williams, O., K., Young, J., Ambient Optomechanical Alignment and Pupil Metrology for the Flight Instruments aboard the James Webb Space Telescope, *Proc. SPIE*, vol. 9195, 2014.
- [13] Kubalak D., Sullivan J., Ohl R., Beaton A., Coulter Ph., Hartig G., Kelley D., Lee D., Maszkiewicz M., Schweiger P., Telfer R., Te Plate M., Wells M., JWST Science Instrument Pupil Alignment Measurements, *Proc. SPIE*, vol 9951, 2016.
- [14] Rohrbach S., O., Kubalak D., A., Gracey R., S, Sabatke D., S, Howard J., M., Telfer R., C., P. Zielinski T.,P., Critical science instrument alignment of the James Webb Space Telescope (JWST) Integrated Science Instrument Module (ISIM), *Proc. SPIE*, vol. 9951 , 2016.